

# Self-Supervised Robustifying Guidance for Monocular 3D Face Reconstruction

Hitika Tiwari<sup>\*†‡</sup> Min-Hung Chen<sup>§</sup> Yi-Min Tsai<sup>§</sup> Hsien-Kai Kuo<sup>§</sup> Hung-Jen Chen<sup>§</sup>

Kevin Jou<sup>§</sup> K. S. Venkatesh<sup>\*</sup> Yong-Sheng Chen<sup>†</sup>

## Abstract

Despite the recent developments in 3D Face Reconstruction from occluded and noisy face images, the performance is still unsatisfactory. One of the main challenges is to handle moderate to heavy occlusions in the face images. In addition, the noise in the face images inhibits the correct capture of facial attributes, thus needing to be reliably addressed. Moreover, most existing methods rely on additional dependencies, posing numerous constraints over the training procedure. Therefore, we propose a Self-Supervised **RO**bstustifying **GU**idance **E** (**ROGUE**) framework to obtain robustness against occlusions and noise in the face images. The proposed network contains 1) the Guidance Pipeline to obtain the 3D face coefficients for the clean faces, and 2) the Robustification Pipeline to acquire the consistency between the estimated coefficients for occluded or noisy images and the clean counterpart. The proposed image- and feature-level loss functions aid the ROGUE learning process without posing additional dependencies. On the three variations of the test dataset of CelebA: rational occlusions, delusional occlusions, and noisy face images, our method outperforms the current state-of-the-art method by large margins (e.g., for the shape-based 3D vertex errors, a reduction from 0.146 to 0.048 for rational occlusions, from 0.292 to 0.061 for delusional occlusions and from 0.269 to 0.053 for the noise in the face images), demonstrating the effectiveness of the proposed approach.

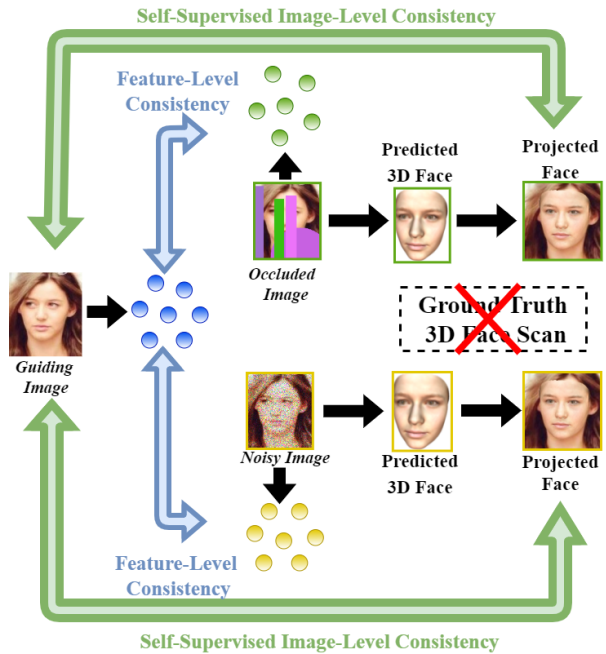


Figure 1. The overview of the proposed *Self-Supervised ROBustifying GUIDance (ROGUE)* framework. ROGUE addresses the occlusion and noise problems in face images for 3D face reconstruction by the proposed image- and feature-level loss functions in the self-supervised fashion, enforcing to occluded and noise coefficients to be consistent with the target coefficients of the guiding image, without the requirement of 3D ground truth face scans and any additional dependency for the training.

## 1. Introduction

3D face reconstruction from monocular face images has been a perennial problem in the field of 3D computer graphics and computer vision. Recent deep-learning-based approaches demonstrate encouraging progress with regards to

perceptual accuracy and training efficiency, facilitating numerous applications such as face recognition [1, 4, 26, 36], face artifice and animation [10, 19, 37]. To address the mathematically ill-posed issue, one of the most common fitting-based methods, *3D Morphable Model (3DMM)* [3], proposes a low-dimensional 3DMM search space spanning the range of human facial appearance. The coordinates from the two sub-spaces, *geometry* and *texture*, along with the illumination and pose parameters generate a 3D face such

<sup>\*</sup>Indian Institute of Technology Kanpur, India

<sup>†</sup>National Yang Ming Chiao Tung University, Taiwan

<sup>‡</sup>Work done during an internship at MediaTek Inc., Taiwan.

<sup>§</sup>MediaTek Inc., Taiwan

that the corresponding face image (projection of 3D face) resembles the target image. However, most of the target images contain occlusions such as glasses, masks, face tattoos, etc. Moreover, face images are usually not noise-free. Therefore, the fitting-based methods may drift the coordinates outside the 3DMM space or distort the 3D face geometry and texture, posing significant challenges to the problem of 3D face reconstruction from monocular face images.

To address the above issues, several approaches have been proposed. Fitting-based optimization approaches [13] iteratively adapt the segmentation map to the target face image. 3D faces can also be obtained from occluded face images using training methodologies with different supervisions [12, 16, 33, 34, 38]. In addition, depth-based methods [22, 39] tackle noise issues for 3D face reconstruction with depth maps. However, the above methods hold several dependencies such as skin masks, depth maps, ground-truth data, synthetic data, segmented maps, multi-images, etc., posing numerous constraints over the training procedure. Therefore, a novel training pipeline that can avoid the above-stated requisites and attain robustness against the facial occlusions and image noise is desired.

In this work, we aim to obtain accurate 3D faces from the occluded and noisy face images with self-supervised learning to eliminate the requirement of 3D ground truth, as shown in Fig. 1. To achieve this goal, we propose a novel *Self-Supervised Robustifying Guidance (ROGUE)* framework, which learns facial statistical coefficients for clean, occluded, and noisy face images simultaneously, and force the estimated coefficients toward clean faces. More specifically, ROGUE contains two parts: 1) The *Guidance Pipeline* estimates coefficients for the clean target face using self-supervised cycle-consistent manners, and 2) the *Robustification Pipeline* enforces the estimated coefficients of occluded and noisy faces to be consistent with clean images. The training is done without additional dependencies by our proposed novel image- and feature-level loss functions. The proposed ROGUE framework is evaluated on three variants of the CelebA [24] dataset (rational occlusions, delusional occlusions, and noise), and outperforms the current state-of-the-art methods by large margins. For example, for the *shape-based* 3D vertex errors, ROGUE achieves a reduction of **67.1%** for rational occlusions, **79.1%** for delusional occlusions, and **80.3%** for the noise in the face images.

In summary, the contributions of our work are three-fold:

1. **Self-Supervised Guidance Pipeline:** We propose a novel pipeline to estimate the facial coefficients for the target face under a self-supervised fashion, eliminating dependencies required by the conventional methods.
2. **Novel Robustification Losses:** We introduce novel image- and feature-level losses such that the occluded and noise coefficients are enforced to be consistent with

the target coefficients, without additional dependencies.

3. **Self-Supervised Robustifying Guidance Framework:** By integrating the *Guidance Pipeline* and *Robustification Pipeline* with robustification losses, the whole **ROGUE** framework can obtain accurate 3D faces by attaining robustness against the challenging facial occlusions and noise in the facial images (e.g., 60+% shape-based vertex error reduction), without 3D ground truth.

## 2. Related Work

**3D Face Reconstruction Methods:** Blanz and Vetter in [3] introduce a morphable model, 3DMM, to facilitate the 3D face modeling, where the obtainment of a set of 3DMM coefficients as a strong prior is critical to reconstructing a 3D face mesh. The fitting-based optimization approaches [2, 3, 14] iteratively optimize the alignment between the target image and the rendered counterpart. The methods in [12, 32, 33, 35] focus on reducing the discrepancies between the face image and the corresponding rendered face. Synthetic data is also adopted [16, 27, 30] as ground-truth labels for training. Recent GAN-based methods [8, 15, 23] also show good accuracy of the 3D reconstructed face. However, the major focus of these methods lies in improving the accuracy of the reconstructed 3D face, where the occlusion and noise issues are not addressed. Moreover, our approach addresses these issues in a self-supervised manner with no dependence upon ground truth and (or) synthetic data for the training.

**Occlusion-Resistive Face Reconstruction:** Egger et al. [13] aim to address the occlusion issues by segmenting the target image into face and non-face regions, and iteratively adapting the face model and the segmentation to the target image. Tran et al. [34] deploy example-based hole filling approach by utilizing the reference set of images containing a suitably similar individual as in the target image. Genova et al. [16] exploit synthetic ground truth data (with the label-free instances of real target image) to tackle the occlusions. Deng et al. [12] train a naive Bayes classifier with Gaussian Mixture Models on a skin image dataset [20] to gain robustness against the occlusions. Yuan et al. [38] exploit 3DMM to tackle the occlusions in 2D images, where the 3D ground truth data obtained by 3DDFA [40] is required.

However, the above methods either only well tackle small-scale occlusions (e.g., minor beards, goggles) instead of large-scale ones (e.g., face masks, tattoos) [12, 13] or rely upon additional dependencies, such as additional images, synthetic data, 3D ground truth, etc. [12, 16, 34, 38]. Instead, our method focuses on tackling the large-scale occlusions without posing additional dependencies.

**Noise-Resistive Face Reconstruction:** The noise in the face images poses a challenge in obtaining accurate 3D

faces. However, to the best of our knowledge, there are no 3D face reconstruction methods [8, 11–13, 15, 16, 23, 31–35] aiming to reconstruct the 3D faces from the heavily noisy face images. There are depth-based methods [22, 39] aiming to address the issues of device-specific noise in obtaining the depth map for reconstructing 3D faces, but tackling the noises in the face images is beyond the scope of those papers. In this paper, the proposed *Self-Supervised Robustifying Guidance framework* aims to attain robustness against the image noise, thus facilitating the accurate reconstruction of 3D faces from noisy monocular face images.

### 3. Technical Approach

We first introduce the preliminaries of the monocular 3D face reconstruction (Section 3.1). Then we present the proposed *Self-Supervised ROBustifying GUIDanceE (ROGUE)* framework (Section 3.2), which addresses the issues of occlusions and face image noise in a self-supervised manner, including the *Guidance Pipeline* (Section 3.2.1) and the *Robustification Pipeline* (Section 3.2.2), as shown in Fig. 2.

#### 3.1. Preliminaries: Monocular Face Reconstruction

In this section, the preliminaries of the proposed approach are introduced, such as 3DMM [3], illumination assumptions, and 3D face projection, crucial to address the problem of 3D reconstruction from monocular face images. **3D Morphable Model (3DMM)**: In 3DMM, a set of geometry and texture coefficients lead to the formation of a 3D face. Thus the formulas of geometry vector  $\mathbf{M}$  and texture vector  $\mathbf{T}$  for the 3DMM model are stated as follows:

$$\mathbf{M} = \overline{\mathbf{M}} + \mathbf{s}\mathbf{B}_s + \mathbf{e}\mathbf{B}_e, \quad \mathbf{T} = \overline{\mathbf{T}} + \mathbf{t}\mathbf{B}_t. \quad (1)$$

A linear combination of  $\mathbf{B}_s \in \mathbb{R}^{3N \times 80}$  and  $\mathbf{B}_e \in \mathbb{R}^{3N \times 64}$  (subsets of Principal Component Analysis basis for shape and expression) with the predicted shape parameter  $\mathbf{s} = [s_1, \dots, s_{80}]$  and expression parameter  $\mathbf{e} = [e_1, \dots, e_{64}]$  respectively morphs the mean 3D face geometry  $\overline{\mathbf{M}} \in \mathbb{R}^{3N}$  (refer to Eq. 1). Similarly, texture morphing is facilitated by adding the mean texture  $\overline{\mathbf{T}} \in \mathbb{R}^{3N}$  to the linear combination of texture basis vector  $\mathbf{B}_t \in \mathbb{R}^{3N \times 80}$  and predicted texture parameter  $\mathbf{t} = [t_1, \dots, t_{80}]$ . The vectors  $\mathbf{B}_t$ ,  $\overline{\mathbf{T}}$ ,  $\mathbf{B}_s$ , and  $\overline{\mathbf{M}}$  are obtained from the Basel Face Model [25] whereas we acquire  $\mathbf{B}_e$  from the Facewarehouse model [6], following [17]. Note that we, as in [12], preclude the ear and neck regions, thus our mesh contains  $N = 36\text{K}$  vertices.

The 3D face illumination is represented using Spherical Harmonics by assuming a *Lambertian* surface reflectance [12]. To obtain the face image, the 3D face coordinates are mapped to the screen by assuming a pinhole camera under full perspective projection, as in [12].

#### 3.2. Self-Supervised Robustifying Guidance

Despite the encouraging results obtained by the previous methods for 3D face reconstruction from occluded face images, there is still a large room for improvement with regards to moderately to heavily occluded face images. In addition, tackling image noise is still an under-addressed issue. Moreover, these methods require several dependencies such as synthetic data, skin mask, etc., posing constraints for training (see Sec. 2 for more details). Therefore, we aim to learn 3D faces in a self-supervised manner without requiring ground truth 3D face scans and other dependencies. To achieve this goal, we propose the *Self-Supervised ROBustifying GUIDanceE (ROGUE)* framework, which is composed of: 1) the *Guidance Pipeline* and 2) the *Robustification Pipeline*. The *Guidance Pipeline* predicts the features from non-occluded face data in a self-supervised fashion (Sec. 3.2.1). The *Robustification Pipeline* takes the *Guidance Pipeline* as the guide and aims to achieve the image- and feature-level consistency with it to address the issues of occlusions and noise in face images (Sec. 3.2.2).

##### 3.2.1 Self-Supervised Guidance Pipeline

One of our main goals is learning reliable 3DMM coefficients with *the least* supervision and dependencies. Inspired by R-Net [12] which contains comparatively fewer dependencies, we propose the **Self-Supervised Guidance Pipeline** to learn the coefficients  $C_G$  by exploiting the cycle-consistency in a self-supervised manner, as shown in Fig. 2 (left). More specifically, the *Guidance Pipeline* takes a clean (i.e., non-occluded noise-free) image  $I_G$  (named *guiding image*) as the input, renders the 3D mesh  $M_G$ , and projects back to get the 2D face image  $I_{G'}$ . And then  $C_G$  is learned by enforcing the consistency between  $I_G$  and  $I_{G'}$ , using only a single monocular face image. Moreover,  $C_G$  guides the Robustification Pipeline (Sec. 3.2.2) to attain robustness against the face occlusions and noise in the images *without relying upon external guidance* such as skin masks [12], synthetic data [16], etc. All the components of the *Guidance Pipeline* are presented as follows:

**Obtaining 3D Face Alignment:** The first consistency that we aim to maintain is the face alignment between the guiding image  $I_G$  and the reconstructed image  $I_{G'}$ , which is achieved by reducing the discrepancy between landmark coordinates of the faces. We represent the discrepancy using the *Landmark Loss*  $\mathcal{L}_K$  as follows:

$$\mathcal{L}_K = \|L_G - L_{G'}\|. \quad (2)$$

where  $L_G$  and  $L_{G'}$  denote a set of 68 landmark coordinates of 2D face image and the rendered counterpart, respectively, and  $\|\cdot\|$  represents the L2 norm.

**Obtaining Photometric Consistency:** To reach the goal of fewer dependencies, we directly regress the pixels of the

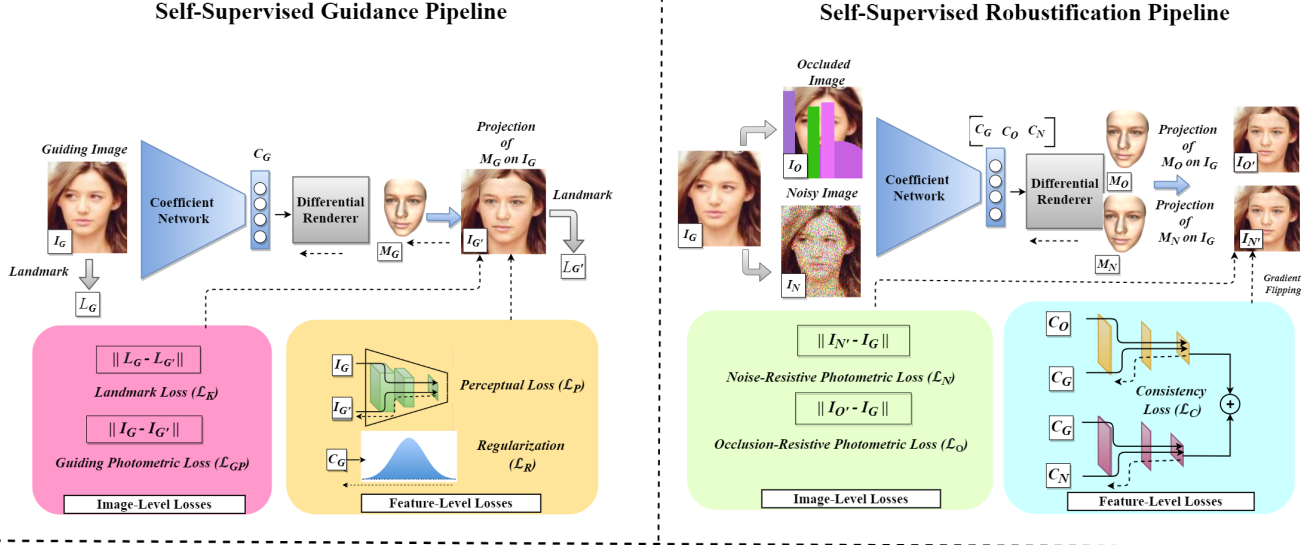


Figure 2. The overall training pipeline of the proposed *Self-Supervised ROBustifying GUIDancE (ROGUE)* framework. The *Guidance Pipeline* (Sec. 3.2.1) ensures the faithful reconstruction of the 3D faces from clean *guiding* images in a cycle-consistent manner, and the *Robustification Pipeline* (Sec. 3.2.2) enforces the estimated coefficients of occluded and noisy images to be consistent with *guiding* images. The training is done in a self-supervised fashion by the proposed image- and feature-level losses, without the need for 3D ground truth.

rendered 3D face ( $I_{G'}$ ) over the corresponding guiding face image ( $I_G$ ), and obtain the pixel-wise consistency between them by the *Guiding Photometric Loss*  $\mathcal{L}_{GP}$  as follows:

$$\mathcal{L}_{GP} = \|I_G - I_{G'}\|. \quad (3)$$

It is worth noting that unlike R-Net [12], we relax the requirement of skin masks as additional dependencies.

**Obtaining Perceptual Loss:** In addition to image-level information, reducing the feature-level discrepancy is also critical to obtaining the perceptual accuracy of 3D faces. Thus, we adopt the *Perceptual Loss*  $\mathcal{L}_P$  as follows:

$$\mathcal{L}_P = 1 - \frac{\langle \theta, \theta' \rangle}{\|\theta\| \|\theta'\|}. \quad (4)$$

where  $\theta$  and  $\theta'$  are the feature representations obtained from the pre-trained FaceNet model [29] for target image  $I_G$  and the corresponding rendered face  $I_{G'}$ , respectively.

**Regularization:** To ensure the plausible face geometry and texture of the reconstructed 3D face, we adopt the *Regularization* term  $\mathcal{L}_R$ , which enforces the coefficients to follow the (normal) distribution of 3DMM, as follows:

$$\mathcal{L}_R = w_s \|s\| + w_t \|t\| + w_e \|e\|, \quad (5)$$

where  $w_s, w_t$  and  $w_e$  are the weights associated with shape  $s$ , texture  $t$ , and expression  $e$  coefficients, respectively.

**Overall Loss for Guidance Pipeline:** The overall loss function  $\mathcal{L}_{guide}$  for the *Self-Supervised Guidance Pipeline* can be expressed below:

$$\mathcal{L}_{guide} = \alpha_K \mathcal{L}_K + \alpha_{GP} \mathcal{L}_{GP} + \alpha_P \mathcal{L}_P + \alpha_R \mathcal{L}_R. \quad (6)$$

where  $\alpha_K, \alpha_{GP}, \alpha_P$ , and  $\alpha_R$  are the weights for landmark loss (Eq. (2)), guiding photometric loss (Eq. (3)), perceptual loss (Eq. (4)) and regularization term (Eq. (5)), respectively. For simplicity, the notation of the image index is ignored throughout the whole paper.

### 3.2.2 Self-Supervised Robustification Pipeline

Although the Guidance Pipeline reduces the requirement of supervision and dependencies, the two major issues for monocular 3D face reconstruction are still not fully addressed: *occlusion* and *noise*. First of all, current methods still cannot well handle the face images with the majority of facial regions occluded, where these methods drift away from their searches from the 3DMM space, resulting in the reconstruction of non-human-like 3D faces. Moreover, additional dependencies such as pre-trained face segmentation model [23], skin masks [12], etc., used by existing methods for tackling the occlusion issues constrain the efficiency of training. Furthermore, despite the progress in the field of 3D face reconstruction, no approach has been proposed to tackle the issue of noise in the face image. All the above challenges motivate the need to learn 3D facial coefficients from occluded and noisy face images more accurately and efficiently. Therefore, we propose the **Self-Supervised Robustification Pipeline** to attain robustness against the occlusions and noise in the face images *with the least additional dependencies*, as shown in Fig. 2 (right). More specifically, We exploit the guiding im-



age  $I_G$  and the estimated coefficients  $C_G$  from Guidance Pipeline (Sec. 3.2.1), and encourage the geometry and texture consistency between the Robustification Pipeline and the Guidance Pipeline, to make  $C_G$  consistent with the estimated coefficients  $C_O$  (from occluded face images  $I_G$ ) and  $C_N$  (from noisy face images  $I_N$ ). All the components of the *Robustification Pipeline* are presented as follows:

**Obtaining Consistency with the Guidance Pipeline:** For obtaining the consistency between the Guidance and Robustification (occlusion and noise) coefficients, we exploit a three-layer Generative Adversarial Network (GAN) architecture and propose the *Consistency Loss*  $\mathcal{L}_C$  as follows:

$$\mathcal{L}_C = \mathcal{L}_{CO} + \mathcal{L}_{CN} \quad (7)$$

$$\mathcal{L}_{CO} = \mathcal{L}_h(\mathcal{D}(C_G, C_O), d_G, d_O) \quad (8)$$

$$\mathcal{L}_{CN} = \mathcal{L}_h(\mathcal{D}(C_G, C_N), d_G, d_N) \quad (9)$$

where  $\mathcal{L}_{CO}$  represents the *occlusion-robustification consistency loss* for tackling the occlusion issues and  $\mathcal{L}_{CN}$  denotes *noise-robustification consistency loss* for tackling the noise in the face image. In both the equations,  $\mathcal{D}$  is the classifier to discriminate  $C_G$  and  $C_i$  ( $i = O/N$ ), and  $\mathcal{L}_h$  denotes the standard Huber loss function. In addition,  $d_i$  ( $i = G/O/N$ ) represents the labels associated with the (guiding/occlusion/noise) coefficients. The *consistency loss* ensures the consistency in perceptual accuracy and alignment between the generated 3D faces for occluded/noisy images and the guiding 3D faces, without requiring 2D landmarks, regularization, pre-trained FaceNet model, and additional 3D ground truth for the training.

**Ensuring the Dominance of Guidance Pipeline:** To ensure that the Robustification Pipeline learns through the experience of Guidance Pipeline and not vice-versa, we directly regress the pixels of the projected 3D face obtained from the occluded face images ( $I_{O'}$ ) and noisy face images ( $I_{N'}$ ) over the guidance counterpart ( $I_G$ ) by the proposed *Occlusion-Resistive Photometric Loss*  $\mathcal{L}_O$  and *Noise-Resistive Photometric Loss*  $\mathcal{L}_N$ , respectively, as follows:

$$\mathcal{L}_O = \|I_{O'} - I_G\|, \quad (10)$$

$$\mathcal{L}_N = \|I_{N'} - I_G\|. \quad (11)$$

**Overall Loss for Robustification Pipeline:** The overall loss function  $\mathcal{L}_{robust}$  for the proposed *Self-Supervised Robustification Pipeline* can be expressed as follows:

$$\mathcal{L}_{robust} = \beta_O \mathcal{L}_O + \beta_N \mathcal{L}_N - \beta_C \mathcal{L}_C \quad (12)$$

where  $\beta_O, \beta_N$  and  $\beta_C$  are the weights associated with occlusion-resistive photometric loss (Eq. (10)), noise-resistive photometric loss (Eq. (11)), and consistency loss (Eq. (7)), respectively. For simplicity, the notation of the image index is ignored here.

It is worth noting that the proposed *Self-Supervised Robustifying Guidance* framework leverages the novel robustification loss function  $\mathcal{L}_{robust}$ . Thus our approach bears a significant difference from R-Net [12] with regards to the model, architecture, loss functions, and the target data. Unlike R-Net, our model does not require skin masks for the training, facilitating the training efficiency. Moreover, our proposed framework is the first (to the best of our knowledge) to tackle the noise in the face images for 3D face reconstruction without 3D ground truth.

## 4. Experiments

In this work, we aim to address the 3D reconstruction problem from occluded and noisy monocular face images without posing additional requirements. To achieve this goal, we create a dataset designed for this problem since there is no publicly available one. For more dataset and implementation details, please refer to the Supplementary.

### 4.1. Dataset

To obtain the training data, we exploit the training set of several standard face datasets, such as 300W-LP [40], LFW [18], LS3D [5], etc. After collecting clean *guiding* images, we create: 1) *delusional occluded* images by overlaying the face images with random shapes of various colors, and 2) *noisy* images by introducing several types of noise with different distributions. To validate the robustness against occlusions and noise, we build three variants of the test set of CelebA [24]: 1) *rational occlusion* set, which refers to real-life occlusions such as goggles, face masks, etc., 2) *delusional occlusion* set, which indicates unrealistic random facial occlusions, and 3) *noisy face* set. For quantitative evaluation, we apply the optimization-based fitting algorithm [3] on clean face testing images to derive correspondent 3D data as the ground truth data. Note that the training and testing datasets are distinct, and the testing data is not accessible during training. As opposed to the recent state-of-the-art methods which utilize 54 subjects, we use 70 subjects to validate the effectiveness and robustness.

### 4.2. Evaluation Metrics

To evaluate the model performance, we use two vertex-based 3D evaluation metrics [12]: *shape-based RMSE vertex error* and *texture-based RMSE vertex error*. The former focuses on deriving the discrepancy between the spatial location of vertices in the reconstructed 3D face and the corresponding ground truth, and the latter compares color consistency between the vertices of the predicted 3D face and the ground truth. Note that each 3D face contains 36K vertices for the comparison with a total of 70 subjects.

### 4.3. Experimental Results

In this section, we show the results on: the 1) *rational occlusion* set, the 2) *delusional occlusion* set, and the 3) *noisy face* set. We compare our results with the several state-of-the-art methods, which focus on monocular 3D face reconstruction beyond full-supervised learning, to investigate how our model reliably tackles the three issues simultaneously. MoFA [33] is the preliminary method proposed to reconstruct 3D faces with occlusion awareness, and R-Net [12] is the best performing model for this problem. For a fair comparison, all the methods reconstruct 3D faces with the same number of face vertices ( $N = 36K$ ), and only the trained CNN-based models (e.g., our coefficient network) are used at the inference stage.

**Rational Occlusions:** Firstly, we investigate the qualitative and the quantitative performance for the *rational occlusions*. We synthetically occlude face images with rational occlusions, such as beards, mustaches, goggles, eye masks, etc., to imitate real-life occlusions. We also show the reconstructed 3D faces from non-occluded images for clearer visual comparisons. In Fig. 3, our method demonstrates better performance than other methods, and is closer to the non-occluded reconstructed 3D faces. Besides, our quantitative results in Table 1 show better vertex and texture-based accuracy for the reconstructed 3D face as compared to other methods. Our proposed method reduces **88.7%** (from 0.425 to 0.048) and **24.6%** (from 0.073 to 0.055) of the shape- and texture-based vertex errors, respectively, from MoFA. In addition, the proposed method reduces **67.1%** ( $0.146 \rightarrow 0.048$ ) and **14.1%** ( $0.064 \rightarrow 0.055$ ) of the shape- and texture-based vertex errors, respectively, from R-Net. All the above results show that the proposed approach tackles the rational occlusions more effectively.

Methods	Vertex Error ( $\downarrow$ )	
	Shape-based	Texture-based
MoFA	$0.425 \pm 0.187$	$0.073 \pm 0.044$
R-Net	$0.146 \pm 0.081$	$0.064 \pm 0.035$
ROGUE (Ours)	<b><math>0.048 \pm 0.006</math></b>	<b><math>0.055 \pm 0.013</math></b>

Table 1. A quantitative comparison of the shape- and texture-based RMSE vertex errors with other approaches for the *rational occlusions*, where the error numbers are the lower the better.

**Delusional Occlusions:** To relax the occlusion types and levels, we build the *delusion occlusion* set by overlaying random shapes and patterns with various colors at random spatial locations on clean face images, leading to much more challenging occlusion conditions than the rational ones. In Fig. 4, previous methods produce unnatural 3D human faces since the predicted coordinates drift away from the 3DMM search space due to severe occlusions. The re-

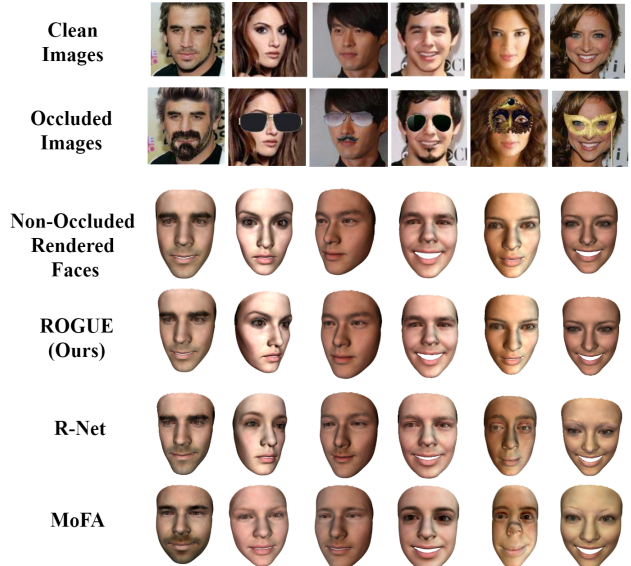


Figure 3. A qualitative comparison of the reconstructed 3D faces with other approaches for the *rational occlusions*. Our results show better robustness against various colors and shapes than other methods, closer to the non-occluded reconstructed 3D faces.

constructed facial colors are also affected by the occlusion colors. Instead, our model restricts the searches to the closest coordinates of the 3DMM space, generating reliable 3D faces. Also, we demonstrate the quantitative efficacy of the proposed method in Table 2. Our proposed method reduces **93.0%** (from 0.872 to 0.061) and **79.8%** (from 0.292 to 0.059) of the shape- and texture-based vertex errors, respectively, from MoFA. In addition, the proposed method reduces **79.1%** ( $0.292 \rightarrow 0.061$ ) and **69.0%** ( $0.197 \rightarrow 0.059$ ) of the shape- and texture-based vertex errors, respectively, from R-Net. All the above results demonstrate that our method is robust even for random heavy occlusions.

Methods	Vertex Error ( $\downarrow$ )	
	Shape-based	Texture-based
MoFA	$0.872 \pm 5.849$	$0.292 \pm 0.314$
R-Net	$0.292 \pm 0.144$	$0.197 \pm 0.096$
ROGUE (Ours)	<b><math>0.061 \pm 0.022</math></b>	<b><math>0.059 \pm 0.013</math></b>

Table 2. A quantitative comparison of the shape- and texture-based RMSE vertex errors with other approaches for the *delusional occlusions*, where the error numbers are the lower the better.

**Noisy Faces:** Finally, we investigate the case of noisy face images by introducing various types of noise such as speckle, salt and pepper, Gaussian, etc. Fig. 9 demonstrates the robustness of the proposed method against the noise in the face images while other methods reconstruct unrealistic 3D faces. In addition, the quantitative results are shown in

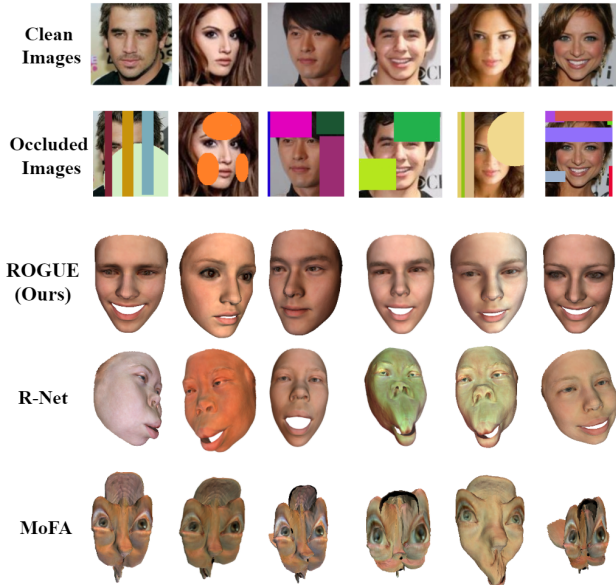


Figure 4. A qualitative comparison of the reconstructed 3D faces with other approaches for the *delusional occlusions*. Our method significantly outperforms others because of the robustness against heavy occlusions with various random colors.

Table 3. Our method reduces **92.8%** (from 0.740 to 0.053) and **74.3%** (from 0.222 to 0.057) of the shape- and texture-based vertex errors, respectively, from MoFA. In addition, the proposed method reduces **80.3%** ( $0.269 \rightarrow 0.053$ ) and **68.7%** ( $0.182 \rightarrow 0.057$ ) of the shape- and texture-based vertex errors, respectively, from R-Net. The above results demonstrate the improvement of our approach.

Methods	Vertex Error ( $\downarrow$ )	
	<i>Shape-based</i>	<i>Texture-based</i>
MoFA	$0.740 \pm 1.462$	$0.222 \pm 0.296$
R-Net	$0.269 \pm 0.112$	$0.182 \pm 0.094$
ROGUE (Ours)	<b><math>0.053 \pm 0.010</math></b>	<b><math>0.057 \pm 0.011</math></b>

Table 3. A quantitative comparison of the shape- and texture-based RMSE vertex errors with other approaches for the *noisy images*, where the error numbers are the lower the better.

#### 4.4. Ablation Study and Analysis

**Impact of Different Losses:** In this paper, we develop an approach to address the problem of various occlusions and noise in the face images. Then a question arises: *Which set of losses is crucial for tackling the aforementioned issues?* To answer this question, we train models with various combinations of the proposed losses and evaluate them using the RMSE vertex errors and average perceptual error. More specifically, the perceptual error is represented by the co-

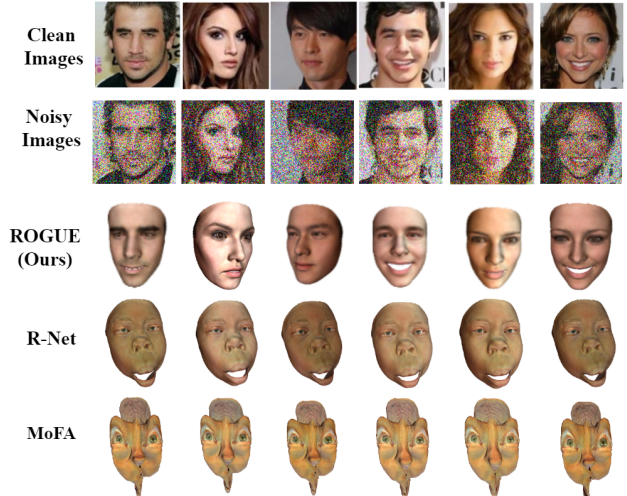


Figure 5. A qualitative comparison of the reconstructed 3D faces with other approaches for the image *noise*. The results show that our method possesses significantly better robustness against the noise in the face images than other approaches. Here we adopt the same noise type and level for a fair comparison.

sine distances between the feature representations obtained using VGGFace2 [7] corresponding to the clean face and the rendered face from rational occluded images.

Table 4 demonstrates the results obtained for the case of *rational occluded* face images.  $\mathcal{L}_O$  and  $\mathcal{L}_N$  alone are not enough to tackle the rational occlusions, and  $\mathcal{L}_C$  is required since it reduces the discrepancy between the guiding coefficients and the predicted delusional and noise coefficients, improving the alignment of the 3D face. A combination of  $\mathcal{L}_O$  and  $\mathcal{L}_N$  only contains the information about the pixel-wise difference between the guiding image and the occlusion-based rendered counterpart. A combination of  $\mathcal{L}_N$  and  $\mathcal{L}_C$  tackles the noise rather than the occlusions. Finally, using all the loss functions leads to the best performance. Due to the page limit, we show the results for the cases of *delusional occlusions* and *noisy images* in the Supplementary, and all the results show that training with all losses ( $\mathcal{L}_O$ ,  $\mathcal{L}_N$ , and  $\mathcal{L}_C$ ) leads to the best performance.

Also, we show the qualitative results in Fig. 6. Without  $\mathcal{L}_C$ , the rendered 3D faces are not reliable. Without  $\mathcal{L}_O$  and  $\mathcal{L}_N$ , the model is not robust to occlusions and noise, respectively. Therefore, it is crucial to deploy  $\mathcal{L}_O$ ,  $\mathcal{L}_N$ , and  $\mathcal{L}_C$  together to achieve the best performance. It is worth noting that the *guiding* coefficients from Guidance Pipeline are also essential to reconstruct reliable and realistic 3D faces.

**Impact of Occlusion Color and Size:** A critical question also arises: *How do colors and sizes of occlusions affect the reconstructed 3D faces?* To answer this, we present a detailed study with various sizes and colors of facial occlusions across the fixed face image. In Fig. 7, it is observed



Losses			Vertex Error ( $\downarrow$ )		Cosine Distance ( $\downarrow$ )
$\mathcal{L}_O$	$\mathcal{L}_N$	$\mathcal{L}_C$	Shape-based	Texture-based	
			0.308	0.082	0.93
✓			0.253	0.076	0.85
	✓		0.298	0.078	0.91
		✓	0.245	0.074	0.70
✓	✓		0.236	0.068	0.84
✓		✓	0.052	0.057	0.42
	✓	✓	0.243	0.071	0.72
✓	✓	✓	<b>0.048</b>	<b>0.055</b>	<b>0.32</b>

Table 4. A quantitative comparison of different loss functions in our framework. In addition to the RMSE vertex errors, we also evaluate the cosine distance between the deep features obtained using VGGFace2 [7] corresponding to the clean face images and the projected counterparts from rational occlusions. The best results (i.e., lowest vertex errors and cosine distance) are obtained when the whole framework is trained using all the losses.

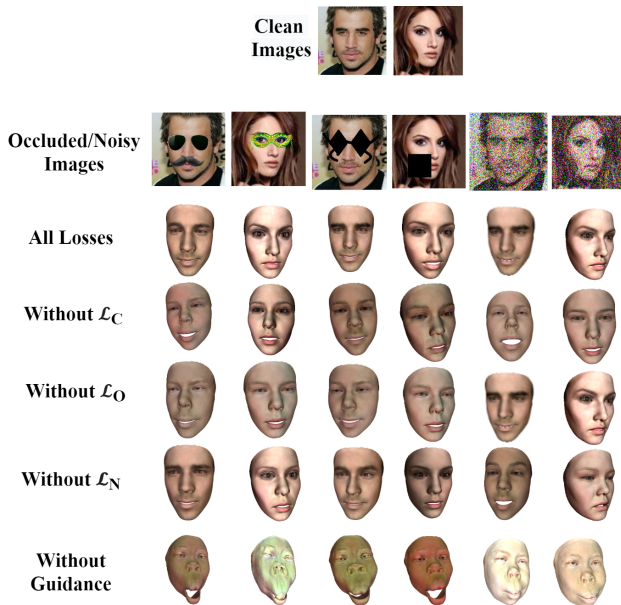


Figure 6. A qualitative comparison of different loss functions in our framework. The results show that all the proposed losses are required to attain full robustness against occlusions and noise.

that our method is highly robust to the sizes of occlusions, and the reconstructed 3D faces are barely affected by the occlusion colors, showing that the proposed model can handle heavily occluded facial regions with varying pixel values.

**Real Occlusions:** To validate the generalization ability of our method, we test our model on real occlusion scenarios rather than the synthesized ones. In Fig. 8, we present various examples to show the robustness of our model towards real-life challenging cases of occlusions in the face images. It is worth noting that the improvement over MoFA and R-Net is more obvious when the occlusion cover more than

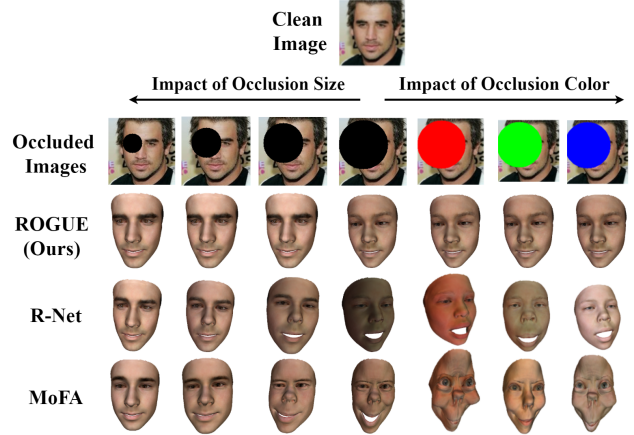


Figure 7. A qualitative comparison of the reconstructed 3D faces with other approaches for different *occlusion sizes and colors*. The results show that the proposed method carries better robustness against various colors and sizes of occlusions.

half of the face and the occlusion is not in skin color.

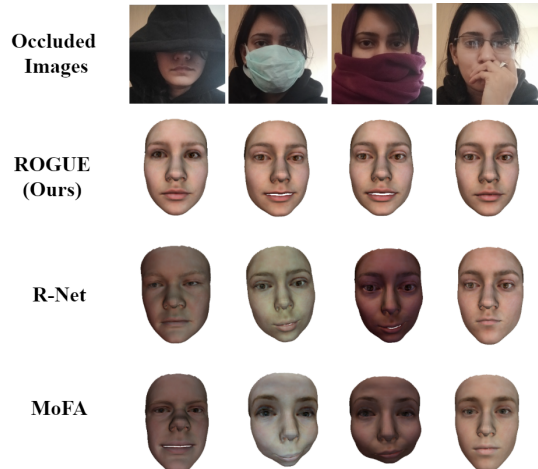


Figure 8. A qualitative comparison for *real occlusions*. The results show that our method is more robust to real heavy occlusions.

**More Discussions:** Due to the page limit, please refer to the Supplementary for: 1) more comparisons with other methods, 2) more ablation studies for the cases of delusional occlusions and noisy images, and 3) the discussions of potential negative societal impact and limitations.

## 5. Conclusions and Future Work

In this work, we propose a novel *Self-Supervised ROBustifying GUIDance (ROGUE)* framework to address the problem of occlusions and noise in the face image for monocular 3D face reconstruction in a self-supervised manner. More specifically, we trained the **Guidance Pipeline**



to guide the **Robustification Pipeline** to see through occlusions (e.g., irrespective of the occlusion colors, shapes, and spatial locations) and noise in the face image. Our experiments indicate that our model outperforms the current state-of-the-art methods by large margins (e.g., for the shape-based 3D vertex error, the *reduction* is **67.1%** for rational occlusions, **79.1%** for delusional occlusions, and **80.3%** for the noise in the face images. For future work, we aim at even fewer training dependencies. For example, We plan to waive the requirement of the Guidance Pipeline by empowering the Robustification Pipeline to self-estimate the probable non-occluded 3D faces that enable the model to gain robustness against the facial occlusions.

## 6. Appendix

In the supplementary material, we would like to show more technical details, experiments, and discussions about the limitations and societal impact.

### 6.1. More Technical Details

**Illumination Model:** To illuminate a 3D face, we assume a *Lambertian* surface reflectance and approximate the face illumination by Spherical Harmonics, following R-Net [12].

$$\mathbf{r}(\mathbf{t}_i, \mathbf{N}_i, \mathbf{\Gamma}) = \mathbf{t}_i \cdot \sum_{b=1}^{B^2} \mathbf{\Gamma}_b \Psi_b(\mathbf{N}_i). \quad (13)$$

Eq. (13) establishes the relationship between radiosity ( $\mathbf{r}$ ) with normal  $\mathbf{N}_i$  of  $i$ -th vertex and texture  $\mathbf{t}_i$  using the coefficient  $\mathbf{\Gamma}_b \in \mathbb{R}^3$  ( $B = 3$  bands) for illuminating the 3D face corresponding to the simple harmonic basis functions such that  $\Psi_b : \mathbb{R}^3 \rightarrow \mathbb{R}$ .

**Projection Model:** A set of vertices  $\mathbf{V}$  of a 3D face are rotated using matrix  $\mathbf{R} \in SO(3)$  and translation vector  $\mathbf{T} \in \mathbb{R}^3$  to obtain the desired 3D face pose.

$$\mathbf{I}' = \zeta(\mathbf{R}^{-1}(\mathbf{V} - \mathbf{T})). \quad (14)$$

In Eq. (14),  $\zeta : \mathbb{R}^3 \rightarrow \mathbb{R}^2$  maps world coordinates.

### 6.2. Experiments

In this section, we detail the datasets and the corresponding variations deployed for training the proposed *Self-Supervised ROBustifying GUIDanceE (ROGUE)* framework (refer to Sec. 6.2.1). In addition, we present the experimental details such as network architecture, weights for the losses, etc., in Sec. 6.2.2. Finally, more experiments for ablation studies are shown in Sec. 6.2.3.

#### 6.2.1 Dataset

For training the ROGUE framework, we exploit the training sets of several datasets such as CelebA [24], 300W-LP [40], LFW [18], and LS3D [5], following R-Net. We

extract clean (non-occluded noise-free) face images from these datasets. In addition, we derive two variants of the images: 1) *delusional occlusions* and 2) *noisy* images. For occluding the face images, we overlay the face images with random shapes of various colors. To generate noisy images we introduce various noise types such as Gaussian, salt and pepper, Poisson, periodic, speckle, etc. Three variations of the face images in the training dataset are served as the input to our training pipeline.

Procuring 3D ground-truth data is difficult due to privacy concerns and monetary issues. Thus to validate the efficacy of the proposed method for obtaining the robustness towards occlusions and image noise, we use three variations of the test dataset of CelebA [24]: *rational occlusion-based*, *delusional occlusion-based*, and *noise-based*. Here the term rational occlusions refer to real-life occlusions such as goggles, face masks, etc., whereas delusional occlusions are unrealistic facial occlusions, including random shapes and colors. Notably, the images in the training and testing datasets are distinct, and we have no access to the test data while training the proposed model. For deriving 3D data corresponding to the images in the test dataset, we run an optimization-based fitting algorithm discussed in [3] on clean face images to obtain 3D ground truth data for evaluation. As opposed to the recent state-of-the-art (utilizing 54 3D subjects), we use 70 such subjects to ensure the effectiveness of the proposed method.

#### 6.2.2 Implementation Details

The proposed *Self-Supervised ROBustifying GUIDanceE (ROGUE)* framework contains a coefficient network and two discriminators to facilitate the self-supervised learning of the model. The coefficient network exploits ResNet-50 as backbone architecture with a modified classification layer by 257 nodes. The face images in the dataset are cropped, aligned (using the method in [9]), and reshaped to size  $224 \times 224$ . These images serve as the input to our model. We opt for a batch of 5 for each case: clean images, occluded faces, and noisy face images. Thus, the proposed network is trained with a net batch size of 15. In addition, we exploit linear GANs with 3 fully-connected layers containing 257, 124, and 2 nodes, respectively in the Robustification Pipeline. Our model is initialized with ImageNet weights [28]. In addition, an Adam optimizer [21] is deployed for training the model with an initial learning rate of  $10^{-4}$  for coefficient network and  $10^{-8}$  for the discriminators. The proposed model contains the *Guidance Pipeline* and the *Robustification Pipeline*, where the weights associated with the losses in Guidance Pipeline are  $\alpha_K = 1.6 \times 10^{-3}$ ,  $\alpha_{GP} = 1.92$ ,  $\alpha_P = 0.2$  and  $\alpha_R = 3 \times 10^{-4}$  (as in R-Net), and the weights for Robustification Pipeline are  $\beta_O = 1.92$ ,  $\beta_N = 1.92$  and

Weights		Vertex Error ( $\downarrow$ )					
$\beta_O$	$\beta_N$	Rational Occlusions		Delusional-Occlusions		Noisy Images	
		Shape-based	Texture-based	Shape-based	Texture-based	Shape-based	Texture-based
0.48	0.48	0.318	0.064	0.334	0.072	0.078	0.059
0.48	1.92	0.300	0.070	0.305	0.070	<b>0.053</b>	<b>0.057</b>
1.62	1.62	0.122	0.061	0.093	0.065	0.062	0.048
1.92	1.92	<b>0.048</b>	<b>0.055</b>	<b>0.061</b>	<b>0.059</b>	<b>0.053</b>	<b>0.057</b>
2.22	2.22	0.13	0.066	0.101	0.069	0.079	0.061
2.84	2.84	0.341	0.068	0.367	0.087	0.083	0.069

Table 5. Impact of weights associated with occlusion- and noise-resistive photometric losses on our results. For this purpose, we fix  $\beta_C = 10^{-3}$ . The table demonstrates the shape-based and texture-based per-vertex RMSE across 70 rational and delusional occlusion-based, and noisy face images on CelebA test dataset.

Weights		Vertex Error ( $\downarrow$ )					
$\beta_C$	Rational-Occlusions		Delusional-Occlusions		Noisy Images		
	Shape-based	Texture-based	Shape-based	Texture-based	Shape-based	Texture-based	
0.0001	0.171	0.056	0.189	0.071	0.076	0.062	
0.001	<b>0.048</b>	<b>0.055</b>	<b>0.061</b>	<b>0.059</b>	<b>0.053</b>	<b>0.057</b>	
0.01	0.186	0.069	0.180	0.068	0.079	0.069	

Table 6. Impact of weights associated with discriminator loss on our results. For this purpose, we fix  $\beta_O = \beta_N = 1.92$ . The table demonstrates the shape-based and texture-based per-vertex RMSE across 70 rational, delusional occlusions-based, and noisy images on CelebA test dataset.

$\beta_C = 10^{-3}$  (please refer to Sec. 6.2.3 are more details).

### 6.2.3 More Ablation Studies

**Choice of Weights for the Losses:** To choose the weights associated with various losses for training the Self-Supervised Robustifying Guidance, we perform several experiments as shown in Tables 5 and 6. In Table 5, we vary the weights  $\beta_O$  and  $\beta_N$  associated with occlusion- and noise-resistive photometric losses by fixing  $\beta_C = 0.001$  corresponding to consistency loss. Besides, to obtain the best performance of the model against the consistency loss, we fix  $\beta_O = \beta_N = 1.92$  and vary the weight  $\beta_C$  in Table 6. Based on the results in the tables, we conclude that the finest performance of the proposed model is obtained at  $\beta_O = \beta_N = 1.92$  and  $\beta_C = 0.001$ .

**Impact of Various Noises:** The proposed Robustification Pipeline enables our model to effectively address the issue of noise in face images. In Fig. 9, we compare our results with R-Net and MoFA for noisy input. The results demonstrate the efficacy of the proposed approach in addressing the issue. It should be noted that MOFA reconstructs reliable 3D face geometry and texture on an average but may generate non-human faces for a few cases. Therefore, the standard deviation holds a very high value corresponding to the 3D error metric shown in Table 3 of the main paper.

**Impact of Various Losses:** In the continuation of the exper-

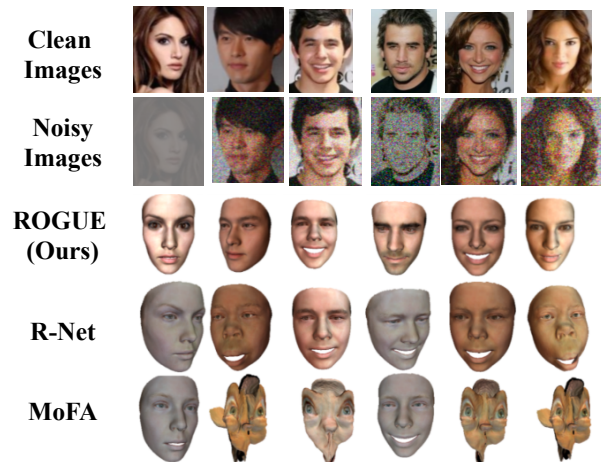


Figure 9. Impact of noisy input on the 3D faces obtained from the proposed method, R-Net, and MoFA.

iments on the impact of losses for the rational occlusions in the main paper, we perform an analysis on the losses for the remaining two cases: *delusional occlusions* and *noisy face images*. Tables 7 and 8 demonstrate the effectiveness of the proposed losses in training our model.

In Table 7,  $\mathcal{L}_O$  is insufficient to tackle delusional occlusions. In addition,  $\mathcal{L}_N$  is not effective for addressing

Losses			Vertex Error ( $\downarrow$ )		Cosine Distance ( $\downarrow$ )
$\mathcal{L}_O$	$\mathcal{L}_N$	$\mathcal{L}_C$	<i>Shape-based</i>	<i>Texture-based</i>	
			0.385	0.094	0.95
✓			0.279	0.083	0.90
	✓		0.359	0.09	0.94
		✓	0.194	0.073	0.79
✓	✓		0.262	0.079	0.89
✓		✓	0.067	0.061	0.41
	✓	✓	0.183	0.072	0.77
✓	✓	✓	<b>0.061</b>	<b>0.059</b>	<b>0.39</b>

Table 7. Shape-based and texture-based Root Mean Squared Error (RMSE) across 70 delusional occlusion-based images on CelebA test dataset. We calculate vertex-to-vertex distance and per-vertex RGB difference between the results and ground truth data obtained by fitting the respective non-occluded subjects.

Losses			Vertex Error ( $\downarrow$ )		Cosine Distance ( $\downarrow$ )
$\mathcal{L}_O$	$\mathcal{L}_N$	$\mathcal{L}_C$	<i>Shape-based</i>	<i>Texture-based</i>	
			0.186	0.073	0.71
✓			0.181	0.069	0.70
	✓		0.094	0.064	0.59
		✓	0.081	0.063	0.47
✓	✓		0.089	0.065	0.56
	✓	✓	0.054	0.060	0.43
✓		✓	0.080	0.062	0.38
✓	✓	✓	<b>0.054</b>	<b>0.060</b>	<b>0.43</b>

Table 8. Shape-based and texture-based Root Mean Squared Error (RMSE) across 70 noisy-face images on CelebA test dataset. We calculate vertex-to-vertex distance and per-vertex RGB difference between the results and ground truth data obtained by fitting the respective clean subjects.

the issue of delusional occlusions. The combination of  $\mathcal{L}_O$  and  $\mathcal{L}_N$  shows no significant improvement in performance. However, the combination of the consistency loss  $\mathcal{L}_C$  and  $\mathcal{L}_O$  improves the 3D vertex accuracy significantly for delusional occlusions. Finally, on exploiting the losses  $\mathcal{L}_O$ ,  $\mathcal{L}_N$  and  $\mathcal{L}_C$  altogether, we obtain the best performance of the proposed model.

For the noisy image, Table 8 shows that the loss  $\mathcal{L}_O$  does not contribute towards the improvement in the model performance. Besides,  $\mathcal{L}_N$  alone is not sufficient to tackle the noise in the face images. An improvement is observed in exploiting  $\mathcal{L}_C$  for training the proposed model. The results demonstrate the best model performance for noisy inputs can be obtained by either deploying a combination of  $\mathcal{L}_C$  and  $\mathcal{L}_N$  or using all the three losses, for example,  $\mathcal{L}_O$ ,  $\mathcal{L}_N$ , and  $\mathcal{L}_C$ . We conjecture that the losses  $\mathcal{L}_O$  and  $\mathcal{L}_N$  are dedicated to addressing the issue of delusional occlusions and noise in the face images, respectively. Thus, no significant improvement can be observed when the three losses are used all together as compared to the grouping of  $\mathcal{L}_O$  and  $\mathcal{L}_C$ , and  $\mathcal{L}_N$  and  $\mathcal{L}_C$  in the case of delusional occlu-

sions and noisy images, respectively. However, their cumulative usage is crucial for real-life scenarios as the face images contain both occlusions and noise.

**Impact of Occlusion Colors:** We present a detailed study on the impact of occlusion color for the reconstructed 3D face. For this purpose, we choose 6 face images and occlude them with a fixed occlusion pattern of red, green, and blue color, as shown in Fig. 10a, 10b, and 10c, respectively. It can be observed that unlike other methods, our approach is highly robust to occlusion colors. In particular, the reconstructed 3D faces in each column (for our case) across red, green, and blue occlusion-based images obtain consistency in the identity of the individual irrespective of occlusion color.

## 6.3. More Discussions

### 6.3.1 R-Net and MoFA on Our Variant Datasets

One question may arise: *What if R-Net and MoFA are also trained using our occluded and noisy images?* Unfortunately, R-Net is unsuitable to get trained on the variant datasets mainly due to the *unreliable skin masks*. While R-Net relies on skin masks to address the issue of occlusions, the delusional occlusions and noise would distort the estimated skin masks, as shown in Fig. 11, and the model may adapt to the occlusions as the facial features. In addition, R-Net exploits the pre-trained face recognition model, FaceNet [29] to obtain the perceptual similarity between the input image and the estimated counterpart. However, FaceNet is trained on rational occlusions, thus poses a challenge for achieving perceptual similarity with delusional occlusions and image noise. Finally, MoFA also demonstrates poor performance when trained on the variant datasets as MoFA does not exploit deep-feature losses that improve the 3D face reconstruction accuracy [12]. More specifically, our Guidance Pipeline is similar to the MoFA framework, and the first row in Table 7 and 8 (where  $\mathcal{L}_O$ ,  $\mathcal{L}_N$ , and  $\mathcal{L}_C$  are all unchecked) demonstrate that the reconstruction errors of the MoFA model trained with the variant datasets are much larger than ours (similar results in Table 4 in the main paper as well). Instead, our **ROGUE** framework can well exploit all the variant data, obtaining a more robust model for 3D face reconstruction.

### 6.3.2 Potential Negative Societal Impact

The proposed method estimates the closest possible 3D face from the occluded and noisy face images. The technology is highly efficient but is not perfect. This may lead to cumbersome situations particularly when used with the face recognition systems for identifying masked criminals at the crime scene. The situation might end up in capturing an innocent person. Along with the above-mentioned impact, invasion of privacy is also a concern with such a technology. The

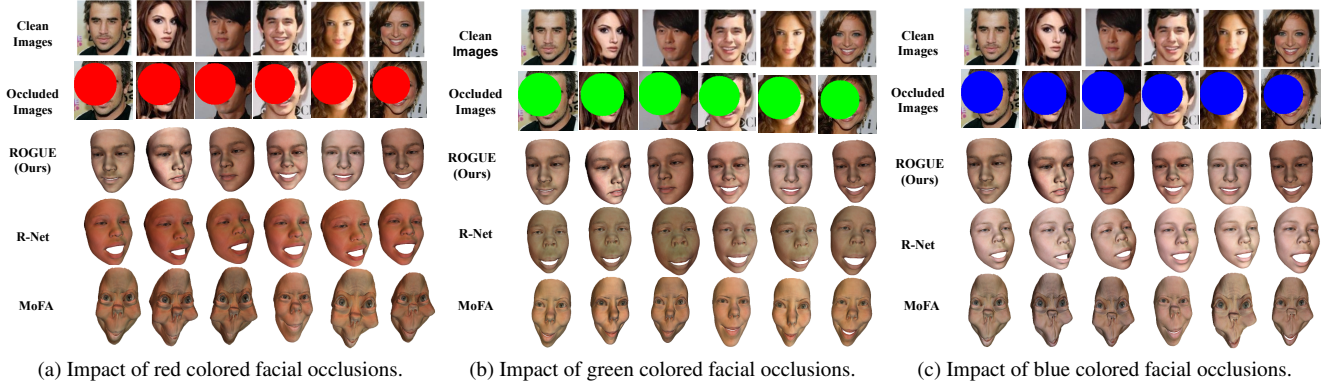


Figure 10. An analysis of the impact of occlusion colors on the reconstructed 3D faces.

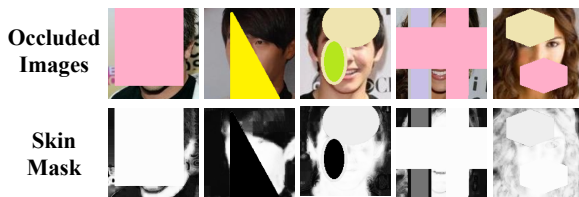


Figure 11. The skin masks obtained for the images in the variant dataset. Note that the skin masks may contain white or near white pixels in the occluded face region, thus leading to inaccurate model learning for 3D face geometry.

estimation of 3D facial data from occluded images might raise concern among those who do not want to reveal their identity in certain situations. The negative impacts may be compensated by boosting the accuracy of the model, by deploying multiple copies of the same face image occluded with different patterns enabling the model to learn the significance of the visible region for reconstructing 3D face geometry and texture.

### 6.3.3 Limitations

The proposed Self-Supervised Robustifying Guidance network addresses the issues of occlusions and noise in monocular face images for reconstructing a 3D face. However, the method requires pre-processing of the images before serving them as the input to Guidance Pipeline and Robustification Pipeline. This increases the net time required for training the proposed model. Further, the automated pre-processing may fail due to several reasons, for example, the inability of the face detection model to detect the face in the image, thus posing a challenge to the proposed approach. This issue may be addressed by deploying domain adaption techniques in which the model learns the 3D face without requiring pre-processed face data. We plan to investigate this direction as our future work.

## References

- [1] Insaf Adjabi, Abdeldjalil Ouahabi, Amir Benzaoui, and Abdelmalik Taleb-Ahmed. Past, present, and future of face recognition: A review. *Electronics*, 9(8):1188, 2020. 1
- [2] Volker Blanz, Curzio Basso, Tomaso Poggio, and Thomas Vetter. Reanimating faces in images and video. *Computer graphics forum*, 22(3):641–650, 2003. 2
- [3] Volker Blanz and Thomas Vetter. A morphable model for the synthesis of 3d faces. In *Proceedings of the 26th annual conference on Computer graphics and interactive techniques*, pages 187–194, 1999. 1, 2, 3, 5, 9
- [4] Volker Blanz and Thomas Vetter. Face recognition based on fitting a 3d morphable model. *IEEE Transactions on pattern analysis and machine intelligence*, 25(9):1063–1074, 2003. 1
- [5] Adrian Bulat and Georgios Tzimiropoulos. How far are we from solving the 2d & 3d face alignment problem?(and a dataset of 230,000 3d facial landmarks). In *Proceedings of the IEEE International Conference on Computer Vision*, pages 1021–1030, 2017. 5, 9
- [6] Chen Cao, Yanlin Weng, Shun Zhou, Yiyong Tong, and Kun Zhou. Facewarehouse: A 3d facial expression database for visual computing. *IEEE Transactions on Visualization and Computer Graphics*, 20(3):413–425, 2013. 3
- [7] Qiong Cao, Li Shen, Weidi Xie, Omkar M Parkhi, and Andrew Zisserman. Vggface2: A dataset for recognising faces across pose and age. In *2018 13th IEEE international conference on automatic face & gesture recognition (FG 2018)*, pages 67–74. IEEE, 2018. 7, 8
- [8] Anpei Chen, Zhang Chen, Guli Zhang, Kenny Mitchell, and Jingyi Yu. Photo-realistic facial details



- synthesis from single image. In *Proceedings of the IEEE/CVF International Conference on Computer Vision*, pages 9429–9439, 2019. 2, 3
- [9] Dong Chen, Gang Hua, Fang Wen, and Jian Sun. Supervised transformer network for efficient face detection. In *European Conference on Computer Vision*, pages 122–138. Springer, 2016. 9
- [10] Qixin Deng, Luming Ma, Aobo Jin, Huikun Bi, Binh Huy Le, and Zhigang Deng. Plausible 3d face wrinkle generation using variational autoencoders. *IEEE Transactions on Visualization & Computer Graphics*, pages 1–1, 2021. 1
- [11] Yu Deng, Jiaolong Yang, Dong Chen, Fang Wen, and Xin Tong. Disentangled and controllable face image generation via 3d imitative-contrastive learning. In *Proceedings of the IEEE/CVF Conference on Computer Vision and Pattern Recognition*, pages 5154–5163, 2020. 3
- [12] Yu Deng, Jiaolong Yang, Sicheng Xu, Dong Chen, Yunde Jia, and Xin Tong. Accurate 3d face reconstruction with weakly-supervised learning: From single image to image set. In *Proceedings of the IEEE/CVF Conference on Computer Vision and Pattern Recognition Workshops*, pages 0–0, 2019. 2, 3, 4, 5, 6, 9, 11
- [13] Bernhard Egger, Andreas Schneider, Clemens Blumer, Andreas Forster, Sandro Schönborn, and Thomas Vetter. Occlusion-aware 3d morphable face models. In *BMVC*, volume 2, page 4, 2016. 2, 3
- [14] Ohad Fried, Eli Shechtman, Dan B Goldman, and Adam Finkelstein. Perspective-aware manipulation of portrait photos. *ACM Transactions on Graphics (TOG)*, 35(4):1–10, 2016. 2
- [15] Baris Gecer, Stylianos Ploumpis, Irene Kotsia, and Stefanos Zafeiriou. Ganfit: Generative adversarial network fitting for high fidelity 3d face reconstruction. In *Proceedings of the IEEE/CVF Conference on Computer Vision and Pattern Recognition*, pages 1155–1164, 2019. 2, 3
- [16] Kyle Genova, Forrester Cole, Aaron Maschinot, Aaron Sarna, Daniel Vlasic, and William T Freeman. Unsupervised training for 3d morphable model regression. In *Proceedings of the IEEE Conference on Computer Vision and Pattern Recognition*, pages 8377–8386, 2018. 2, 3
- [17] Yudong Guo, Jianfei Cai, Boyi Jiang, Jianmin Zheng, et al. Cnn-based real-time dense face reconstruction with inverse-rendered photo-realistic face images. *IEEE transactions on pattern analysis and machine intelligence*, 41(6):1294–1307, 2018. 3
- [18] Gary B Huang, Marwan Mattar, Tamara Berg, and Eric Learned-Miller. Labeled faces in the wild: A database for studying face recognition in unconstrained environments. In *Workshop on faces in 'Real-Life' Images: detection, alignment, and recognition*, 2008. 5, 9
- [19] Zihao Jian and Minshan Xie. Realistic face animation generation from videos. *arXiv preprint arXiv:2103.14984*, 2021. 1
- [20] Michael J Jones and James M Rehg. Statistical color models with application to skin detection. *International journal of computer vision*, 46(1):81–96, 2002. 2
- [21] Diederik P Kingma and Jimmy Ba. Adam: A method for stochastic optimization. In *International Conference on Learning Representations (ICLR)*, 2015. 9
- [22] Peixin Li, Yuru Pei, Yicheng Zhong, Yuke Guo, and Hongbin Zha. Robust 3d face reconstruction from single depth image through semantic consistency. *IET Computer Vision*, 2021. 2, 3
- [23] Jiangke Lin, Yi Yuan, Tianjia Shao, and Kun Zhou. Towards high-fidelity 3d face reconstruction from in-the-wild images using graph convolutional networks. In *Proceedings of the IEEE/CVF Conference on Computer Vision and Pattern Recognition*, pages 5891–5900, 2020. 2, 3, 4
- [24] Ziwei Liu, Ping Luo, Xiaogang Wang, and Xiaoou Tang. Deep learning face attributes in the wild. In *ICCV*, pages 3730–3738. IEEE Computer Society, 2015. 2, 5, 9
- [25] Pascal Paysan, Reinhard Knothe, Brian Amberg, Sami Romdhani, and Thomas Vetter. A 3d face model for pose and illumination invariant face recognition. In *2009 sixth IEEE international conference on advanced video and signal based surveillance*, pages 296–301. Ieee, 2009. 3
- [26] Nick Pears and Ajmal Mian. 3d face recognition. In *3D Imaging, Analysis and Applications*, pages 569–630. Springer, 2020. 1
- [27] Elad Richardson, Matan Sela, and Ron Kimmel. 3d face reconstruction by learning from synthetic data. In *2016 fourth international conference on 3D vision (3DV)*, pages 460–469. IEEE, 2016. 2
- [28] Olga Russakovsky, Jia Deng, Hao Su, Jonathan Krause, Sanjeev Satheesh, Sean Ma, Zhiheng Huang, Andrej Karpathy, Aditya Khosla, Michael Bernstein, et al. Imagenet large scale visual recognition challenge. *International journal of computer vision*, 115(3):211–252, 2015. 9
- [29] Florian Schroff, Dmitry Kalenichenko, and James Philbin. Facenet: A unified embedding for face recognition and clustering. In *Proceedings of the IEEE con-*

- ference on computer vision and pattern recognition*, pages 815–823, 2015. 4, 11
- [30] Matan Sela, Elad Richardson, and Ron Kimmel. Unrestricted facial geometry reconstruction using image-to-image translation. In *Proceedings of the IEEE International Conference on Computer Vision*, pages 1576–1585, 2017. 2
- [31] Ayush Tewari, Mohamed Elgharib, Gaurav Bharaj, Florian Bernard, Hans-Peter Seidel, Patrick Pérez, Michael Zollhofer, and Christian Theobalt. Stylerig: Rigging stylegan for 3d control over portrait images. In *Proceedings of the IEEE/CVF Conference on Computer Vision and Pattern Recognition*, pages 6142–6151, 2020. 3
- [32] Ayush Tewari, Michael Zollhöfer, Pablo Garrido, Florian Bernard, Hyeonwoo Kim, Patrick Pérez, and Christian Theobalt. Self-supervised multi-level face model learning for monocular reconstruction at over 250 hz. In *Proceedings of the IEEE Conference on Computer Vision and Pattern Recognition*, pages 2549–2559, 2018. 2, 3
- [33] Ayush Tewari, Michael Zollhofer, Hyeonwoo Kim, Pablo Garrido, Florian Bernard, Patrick Perez, and Christian Theobalt. Mofa: Model-based deep convolutional face autoencoder for unsupervised monocular reconstruction. In *Proceedings of the IEEE International Conference on Computer Vision Workshops*, pages 1274–1283, 2017. 2, 3, 6
- [34] Anh Tuan Tran, Tal Hassner, Iacopo Masi, Eran Paz, Yuval Nirkin, and Gérard G Medioni. Extreme 3d face reconstruction: Seeing through occlusions. In *CVPR*, pages 3935–3944, 2018. 2, 3
- [35] Luan Tran and Xiaoming Liu. Nonlinear 3d face morphable model. In *Proceedings of the IEEE conference on computer vision and pattern recognition*, pages 7346–7355, 2018. 2, 3
- [36] Anh Tuan Tran, Tal Hassner, Iacopo Masi, and Gérard Medioni. Regressing robust and discriminative 3d morphable models with a very deep neural network. In *Proceedings of the IEEE conference on computer vision and pattern recognition*, pages 5163–5172, 2017. 1
- [37] Dan Ye and Chiou-Shann Fuh. 3d morphable face model for face animation. *International Journal of Image and Graphics*, 20(01):2050003, 2020. 1
- [38] Xiaowei Yuan and In Kyu Park. Face de-occlusion using 3d morphable model and generative adversarial network. In *Proceedings of the IEEE/CVF International Conference on Computer Vision*, pages 10062–10071, 2019. 2
- [39] Yicheng Zhong, Yuru Pei, Peixin Li, Yuke Guo, Gengyu Ma, Meng Liu, Wei Bai, WenHai Wu, and Hongbin Zha. Face denoising and 3d reconstruction from a single depth image. In *2020 15th IEEE International Conference on Automatic Face and Gesture Recognition (FG 2020)*, pages 117–124. IEEE, 2020. 2, 3
- [40] Xiangyu Zhu, Zhen Lei, Xiaoming Liu, Hailin Shi, and Stan Z Li. Face alignment across large poses: A 3d solution. In *Proceedings of the IEEE conference on computer vision and pattern recognition*, pages 146–155, 2016. 2, 5, 9